

Contact lens holographic projection display based on curved volume-holographic optical element

Jin Su Lee 

Digital Holography Research Section,
Electronics and Telecommunications
Research Institute, Daejeon, Republic of
Korea

Correspondence

Jin Su Lee, Digital Holography Research
Section, Electronics and
Telecommunications Research Institute,
Daejeon, Republic of Korea.
Email: jslee27@etri.re.kr

Funding information

Institute of Information &
communications Technology Planning
(IITP) grant funded by the Korea
government (MSIT), Grant/Award
Number: 2020-0-01842; Electronics and
Telecommunications Research Institute
(ETRI) grant funded by the Korean
government (MIST), Grant/Award
Number: 23ZH1300; Korean government
(MIST), Grant/Award Numbers:
23ZH1300, 2020-0-01842

Abstract

Wearable devices for augmented reality (AR) have gained considerable attention but research on contact lenses remains scarce. This study introduces an AR display that utilizes a contact lens integrated with a holographic projection display and a curved volume-holographic optical element. We designed a holographic projection display with a total FoV 15°(supported FoV 10°) and a 6.9 mm × 3.9 mm eyebox, respectively. The computer-generated hologram was optimized to null quality degradation caused by pupil constraints and asymmetric diffraction efficiency distribution. The diffraction efficiency of the holographic optical element used in the contact lens was calculated to provide insights into the anticipated optical performance and identify issues associated with the proposed system. Excellent performance with a maximum diffraction efficiency of 95% is demonstrated under Bragg conditions. However, a substantial drop in efficiency is observed at angular deviations 4°. Conversely, the wavelength deviations had a negligible impact on diffraction efficiency. Finally, the proposed contact lens holographic display was optically reconstructed, confirming its potential as a next-generation wearable display technology.

KEYWORDS

augmented reality, contact lenses, holography, volume-holographic optical element

1 | INTRODUCTION

Conventionally, contact lenses have been used to correct visual impairments such as myopia, hyperopia, and astigmatism. Contact lenses are among the most extensively used wearable devices. Currently, smart contact lenses are being developed to monitor health conditions, such as dry eye disease, intraocular eye pressure, and glucose levels. However, research on contact lens displays is rare. To the best of our knowledge, it is difficult to obtain a sufficient field of view (FoV) and eyebox because contact

with the pupil has very short optical path length. Therefore, conventional augmented reality (AR) optical structures cannot be used as contact lenses, directly. To overcome these obstacles, we firstly applied a holographic projection display to a contact lens in this study. Holographic displays have received considerable attention for use in a variety of fields, including automobile, military, and medical applications [1]. Digital holographic display technology has already been applied to AR display applications [2–5] because it can provide a natural three-dimensional (3D) experience without

vergence-accommodation conflict. Nevertheless, we have no idea of a contact lens holographic display because most wearable AR displays are built into glasses or goggles; hence, they all require a bulky and wide-beam coupler (such as a beam splitter, diffractive optical element, holographic optical element, freeform lens, or meta-lens) to transfer the image to the eyes [6, 7]. In addition, to correct myopia, hyperopia, and astigmatism, glasses or helmet-type AR displays should include additional optics, which increase weight, cost and inconvenience. In contrast, contact lenses can provide extraordinary convenience for daily use in sports and outdoor life [8, 9].

Moreover, they provide precise vision without magnification because they are in contact with the pupil. Nevertheless, it is very difficult to apply optical component directly on a contact lens surface. A contact lens has a small surface area and is too thin to allow the insertion or engraving of an optical component inside the material. As far as our knowledge, we did not find any similar researches about contact lens holographic display based on a holographic projection optics. Additionally, proposed research diverges from previous studies by opting for a separated system, rather than directly embedding the display panel and circuitry into the contact lens. This decision takes into account factors such as feasibility and stability, marking a pivotal distinction in our approach compared with prior research [10, 11]. Therefore, we believe that holographic display technology is the best candidate for the advanced contact lens displays. Previous studies on contact lens displays were approached as an all-in-one concept, meaning that a light source, battery, circuits, and optics designed to have geometrical optical structures were applied directly to the contact lens.

The main objective of this research is to validate the potential applications of holographic displays in contact lenses as shown in Figure 1. Furthermore, we indirectly establish the applicability of the proposed study to holographic displays with complex structures beyond contact

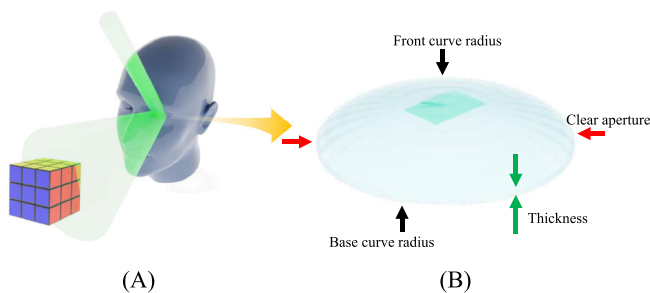


FIGURE 1 (A) Three-dimensional (3D) modeling of the proposed idea and (B) contact lens with curved volume-holographic optical element.

lenses, through the following details: (i) analysis of the diffraction efficiency of curved transmissive HOE components; (ii) configuration of a contact lens holographic display system; and (iii) introduction to CGH optimization for compensating diffraction efficiency imbalances. As far as our knowledge, this proposed research is the first of its kind and stands as a rare study enabling the observation of holograms through contact lenses.

2 | PROPOSED METHOD

2.1 | Diffraction efficiency analysis in curved volume-holographic optical element

To calculate the diffraction efficiency($\eta(x,y)$) of a curved surface as shown in Figure 2, the angle between two vectors in an arbitrary space is needed to define the incident and diffracted beams using the dot product of the vectors as indicated by (1).

$$\theta = \arccos \frac{\vec{o}_n \cdot \vec{n}_n}{\|\vec{o}_n\| \|\vec{n}_n\|}, \quad \phi = \arccos \frac{\vec{r}_n \cdot \vec{n}_n}{\|\vec{r}_n\| \|\vec{n}_n\|}. \quad (1)$$

The object wave vector \vec{o}_n , surface normal vector \vec{n}_n , and reference wave vector \vec{r}_n are required at each local point. The Kogelnik's coupled wave theory provides a formula for calculating the diffraction efficiency of volumetric holographic optical element (HOE). However, this formula assumes that the HOE is planar. Therefore, to calculate the diffraction efficiency of a HOE with

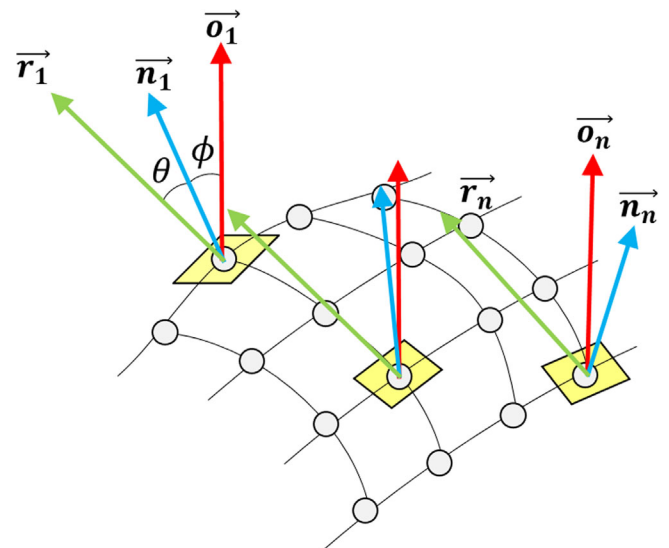


FIGURE 2 Normal vectors at freeform surface.

curvature, it is necessary to compute the object and reference beam relationships based on the normal vector of the unit plane. This process is performed for all unit planes according to (2), and by iterating through this procedure, it becomes possible to calculate the diffraction efficiency of a transmissive HOE with curvature [12].

Additionally, the diffraction efficiency equation for volume HOE varies depending on their thickness and differs in the cases of reflective and transmissive types. In this study, because the Q parameter that determines the volume satisfies the volume requirements and a transmissive element was used, the reflective types were not considered. Therefore, the diffraction efficiency $\eta(x,y)$ of transmissive volume-holographic optical element can be calculated as follows:

$$\eta(x,y) = \frac{\sin^2\left(\sqrt{\nu^2(x,y) + \xi^2(x,y)}\right)}{1 + \frac{\xi^2(x,y)}{\nu^2(x,y)}} \quad (2)$$

where the parameters ν and ξ are given by

$$\nu(x,y) = \frac{\pi n_1 d}{\sqrt{\lambda^2 \cos^2 \theta(x,y) - \frac{K \lambda^2 \cos \theta(x,y) \cos \phi(x,y)}{2\pi n_0}}} \quad (3)$$

and

$$\xi(x,y) = \frac{\Delta \theta K \sin(\phi(x,y) - \theta(x,y)) d - \frac{\Delta \lambda K^2 d}{4\pi n_0}}{2 \cos \theta(x,y) - \frac{K \lambda \cos \phi(x,y)}{\pi n_0}} \quad (4)$$

where η_m is the diffraction efficiency of each local point, n_1 is the index perturbation, d is the thickness of the recording layer, λ is the wavelength of light in vacuum, θ is the angle of the reference beam and surface normal, and ϕ is the angle of the diffracted beam and surface normal; K is the grating number, Λ is the grating period, n_0 is the bulk index of the material, $\Delta \lambda$ is the wavelength deviation of the incident beam, and $\Delta \theta$ is the angular deviation of the incident beam. Thus, based on the above equations, the diffraction efficiency of diffractive optical elements can be calculated using aspheric or freeform surfaces as shown in Figure 3. In the element's area, increasing the number of points to calculate the diffraction efficiency improves the accuracy; however, we calculated 8 294 400 points, which corresponded to the physical pixel resolution of the used SLM.

Although the angles of the incident and diffracted beams were fixed, the diffraction efficiency changed gradually because the surface normal vector changed continuously. In particular, because contact lenses typically cause changes in the front curve radius for vision

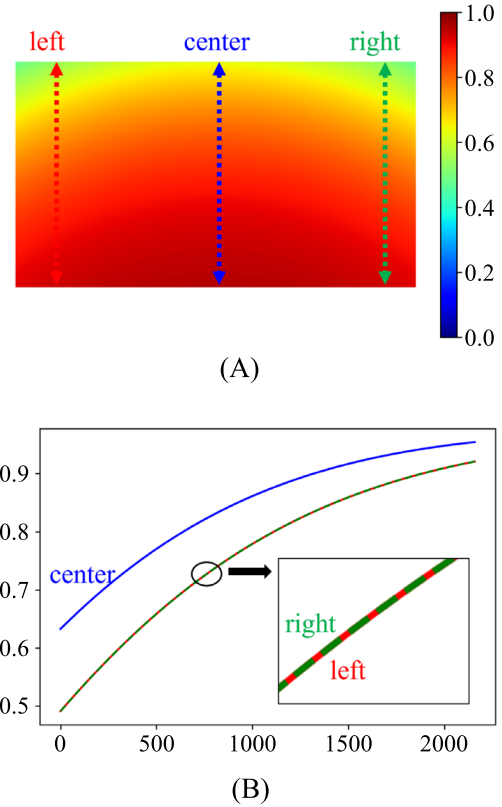


FIGURE 3 Calculated diffraction efficiency distribution of curved volume-holographic optical element. (A) 3D plot, (B) top view, (C) cross-section of data for left, center, and right positions.

correction, the diffraction efficiency can vary according to the corrective ability of the contact lens. In this study, the diffraction efficiency was calculated when the front curve radius (R) was changed from 7.28mm to 10.65mm corresponding to dioptric powers ranging from 9.5D to $-9.5D$. As shown in Figure 4, a smaller front curve radius results in rapid changes in diffraction efficiency, thus making it difficult to achieve a uniform intensity distribution of the hologram. However, a larger front curve radius reduces the degree of change in the diffraction efficiency over the entire area. That is, it has the advantage of achieving a uniform intensity distribution over the entire area.

Although theoretically the highest diffraction efficiency is obtained when the Bragg condition is satisfied, in reality, there is a significant deviation from theory. Among these, the wavelength deviation and incident angle deviation are the primary causes of the reduction in the diffraction efficiency. To verify this, simulations were conducted to observe the changes in the diffraction efficiency when angle deviations of 0° , 2° , and 4° were introduced when R was 7.28 mm as shown in Figure 5. The diffraction efficiency decreases as the angular deviation increases, and when the deviation reaches 4° , the

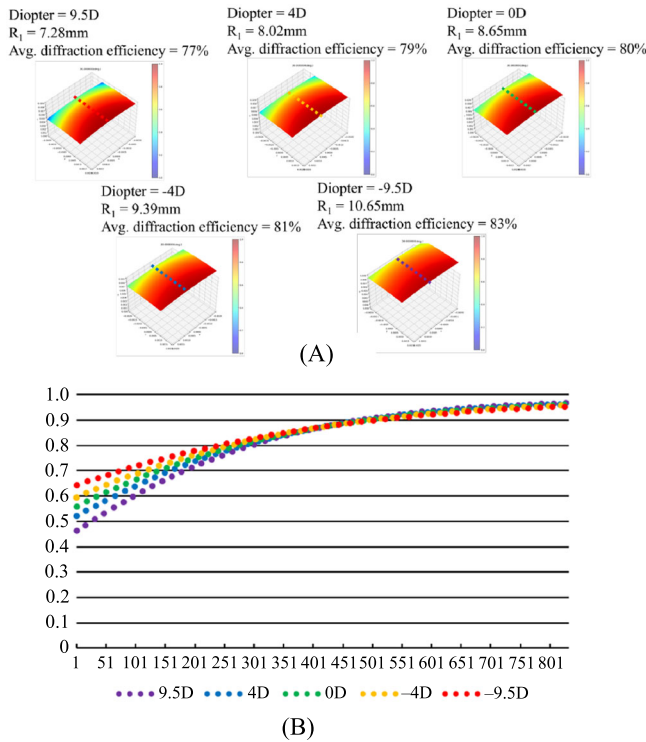


FIGURE 4 Three-dimensional distributions of diffraction efficiency and cross-sectional plots depending on the front curve radius (A) 7.28 mm (9.5D), (B) 8.02 mm (4D), (C) 8.65 mm (0D), (D) 9.30 mm (−4D), and (E) 10.65 mm (−9.5D).

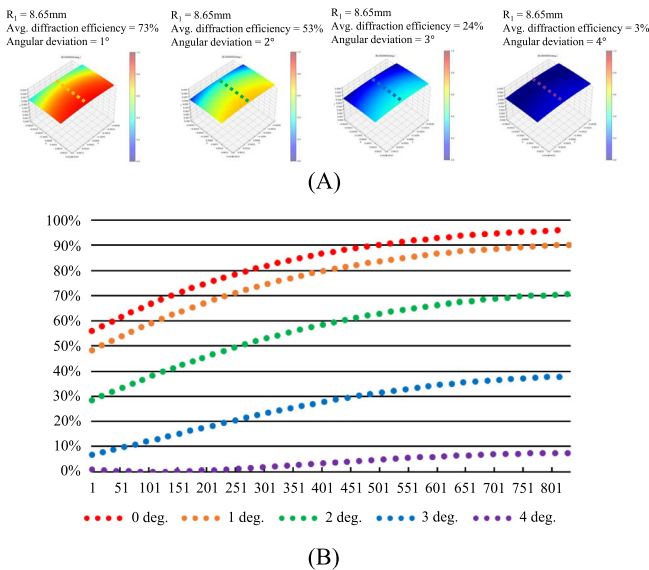


FIGURE 5 (A) Three-dimensional distributions of diffraction efficiency depending on the angular deviation (1° to 4°) and (B) cross-sectional plots of data in (A).

overall average diffraction efficiency falls below 10%. The maximum diffraction efficiency (marked as Max. D. E.) also decreases by 7.2% at a 4° deviation, as shown in

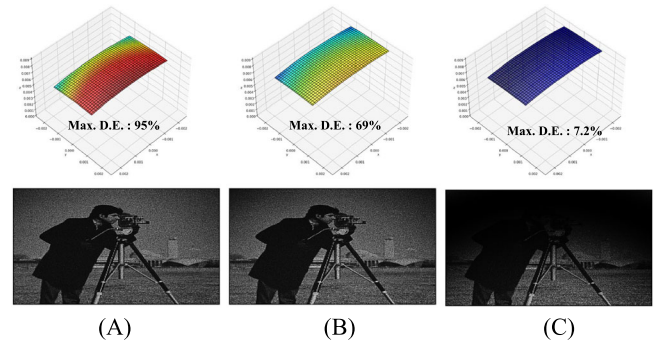


FIGURE 6 Reproduced hologram images depending on the diffraction efficiency distribution.

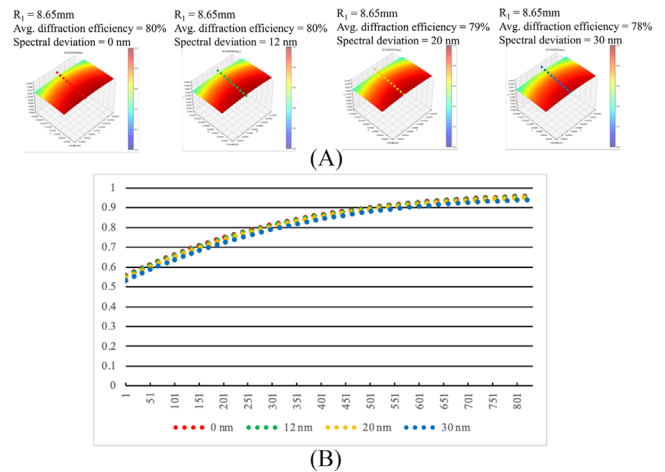


FIGURE 7 Three-dimensional distributions of diffraction efficiency depending on the wavelength deviation (A) from 0 nm to 20 nm, and (B) cross-sectional plots of data in (A).

Figure 6. Therefore, it can be expected that a problem arises with the proposed contact lens display as the wearers need to keep their heads and eyes still.

Simulations were conducted based on the changes in the intensity of the hologram reproduction image owing to the variation in the diffraction efficiency caused by the deviation of the incident angle. When the angular deviation reached 2°, the hologram image began to darken, starting from the upper corners. At 4°, more than half of the images were barely visible. Although the hologram images shown in the simulation appear at an observable level owing to normalization, the actual hologram-reproduced image quality is expected to be poorer owing to optical aberrations, laser speckle, and other issues.

In contrast, the change in the diffraction efficiency due to the wavelength deviation was minimal, as shown in Figure 7. In other words, transmissive volume-holographic optical elements have poor wavelength selectivity, confirming that the choice of light sources for

incident beams is limited. However, as previously described, they exhibit excellent angular selectivity, thus indicating their potential in optical designs to minimize the effects of external light sources. The experiments were conducted in an indoor environment to validate the proposed method.

2.2 | Fabrication of a curved volume-holographic element

A film-type volume-holographic optical element (Bayfol HX200) was used in this experiment. This is because film-type volume-holographic optical elements can be easily handled and attached to curved surfaces without complicated coating processes. The contact lens used in this study is a rigid gas-permeable lens with a 10 mm diameter and 8.5 mm peripheral curve radius. In the experiment, the film-type volume-holographic optical element was cut to a size of 5 mm × 2.5 mm size, and was then attached to the contact lens surface with an optical adhesive, as shown in Figure 8. The properties of the curved volume-holographic optical element, which deflects the beam off-axis and records the conditions, are summarized in Table 1.

The laser light source had a wavelength of 532 nm, and the power of each beam was 15 mW with an exposure time of 60 s. Subsequently, the substrate was bleached for 30 s using an ultraviolet (UV) lamp. In the

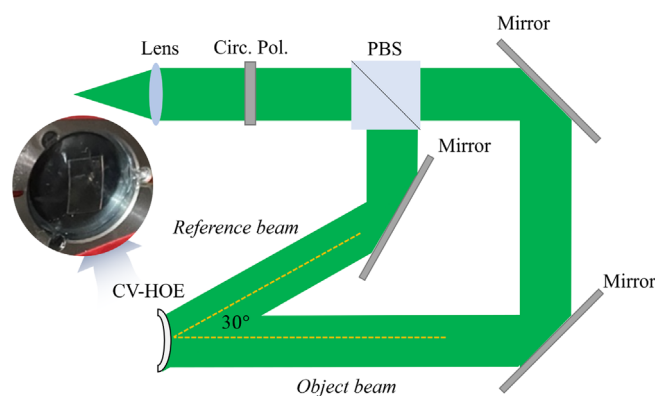


FIGURE 8 Schematic of optical system of volume-holographic optical element recording.

TABLE 1 Recording condition details.

Film thickness	16 μm
Exposure time	60 s
Total exposure energy	500 mJ
Bleaching time	30 s

optical recording system, the reference beam angle for the V-HOE was set to 30°, and the object beam angle was set to 0°. The exposure time was controlled by using an electric shutter. The laser light source had a wavelength of 532 nm, and the power of each beam was 15 mW with an exposure time of 60 s. Subsequently, the substrate was bleached for 30 s using a UV lamp. In the recording optical system, the reference beam angle for the curved volume-holographic optical element was set to 30°, and the object beam angle was set to 0°.

3 | EXPERIMENTAL RESULTS

3.1 | Optical system of proposed holographic display

The recorded curved volume-holographic optical element was attached to the front surfaces of the contact lenses using an optical adhesive as shown in Figure 8. Although the film-type, volume-holographic optical element is thick owing to its substrate layer, it is easy to handle and fabricate, thus avoiding the complicated coating processes mentioned above. The fabricated contact lens, which is a passive component without electrical parts, functions solely to deflect light toward the retina. Therefore, a holographic projector was required to transmit the hologram from the spatial light modulator. As depicted in Figure 9A, the light reflected from the LCOS-SLM passes through the first set of 4F optics to increase the FoV and eliminate DC noise. Subsequently, it travels through a second set of 4F optics to deliver the hologram to the pupil. Consequently, the digital holographic projector has an exit pupil size of 6.9 mm × 3.9 mm and an approximate FoV of 15°. A full-color laser diode emitting at the wavelengths of 420 nm, 520 nm, and 632 nm, is

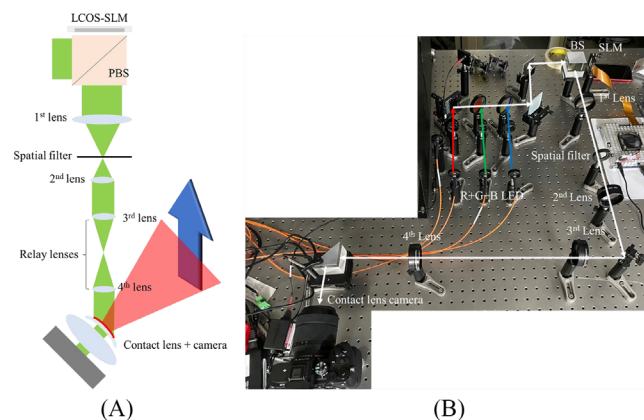


FIGURE 9 (A) Schematic of the simplified optical structure of the proposed contact lens augmented reality display and (B) experimental setup on the optical table.

employed, but the device was designed only for green wavelengths. To demonstrate its feasibility, blue and red hologram images were also captured, even though they exhibited size distortion. The focal lengths of the 1st, 2nd, 3rd, and 4th lenses are 200 mm, 100 mm, 200 mm, and 200 mm, respectively.

3.2 | Optimized computer-generated hologram for intensity uniformity

Creating a computer-generated hologram (CGH) for the proposed holographic projection display is straightforward. In contrast to the angular spectrum method, holographic projection displays employ the inverse Fourier transform. Therefore, the depth of the hologram image can be represented by performing a Fourier transform on any image signal and multiplying it by a quadratic phase. This can be expressed by (5).

$$U_1(x, y) = e^{\frac{i\pi}{\lambda}(x^2+y^2)} \mathbf{FT}[U_0(u, v)]. \quad (5)$$

The symbol **FT** stands for Fourier Transform. The symbols λ and f denote the wavelength and distance from the object plane $U_0(u, v)$ to the hologram plane $U_1(x, y)$, respectively.

Holographic projection displays the position of the pupil within the eyebox and observes the hologram, which causes the pupil to act as a bandpass filter limiting the CGH signal. This degrades the quality of the reproduced hologram. In this study, LCOS-SLM has a $3.6 \mu\text{m}$ pixel pitch and $13.8 \text{ mm} \times 7.8 \text{ mm}$. However, because the proposed curved volume-holographic optical element has a size of $5 \text{ mm} \times 2.5 \text{ mm}$ and the pupil has only a 4 mm diameter, if the holographic projector delivers the hologram without resizing the pixel pitch, half of the CGH signal is cut off, as shown in Figure 10A. However, if the SLM has a $1.8 \mu\text{m}$ pixel pitch and a size of

$6.9 \text{ mm} \times 3.9 \text{ mm}$, it utilizes the entire spatial bandwidth, as illustrated in Figure 10B. Although the exit pupil size (equal to the eyebox) was smaller than before, the peak signal-to-noise ratio of the hologram image improved by 1.5 dB and the FoV expanded from 7.5° to 15° .

The generated CGH mentioned earlier used the conventional method. As I mentioned above section, such as the pupil acting as a band-pass filter, and uneven brightness owing to changes in diffraction efficiency (as indicated in Section 2.1) directly affect the quality of the hologram. To compensate for these issues, it is necessary to either improve the structure of the holographic optical element or optimize the CGH. Improving the structure of the holographic optical element can be an optical enhancement method that reduces the computational load of CGH; unfortunately, it is very challenging to manufacture because of the extremely low thickness ($80 \mu\text{m}$) of the contact lenses. Therefore, optimizing the CGH is more effective and economical for improving the quality of the hologram images. For this purpose, an optimized CGH was generated based on the Adam optimizer by following the flowchart in Figure 11, considering two variables: the pupil diameter and angle of the incident beam, thus improving the image quality. The pupil size was based on a standard size of 4 mm, and the optimized CGH was extracted for the diffraction efficiency distribution at a front curve radius of 8.65 mm (0D) when the incident angles were 0° , 1° , 2° , and 3° . A flowchart of the algorithm used is shown in Figure 11, and the input image used was an image of DIV2 K datasets.

The results of the optimization are shown in Figure 12. In the figure, the horizontal axis represents the angular deviation, and the vertical axis, from top to bottom, indicates the diffraction efficiency distribution, hologram image before optimization, hologram image after optimization, and the optimized CGH, respectively. Through the optimization process of the proposed method, it is evident that the brightness distribution of

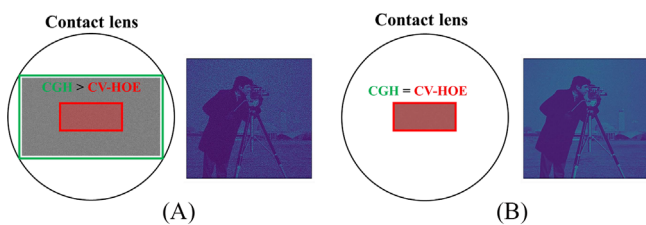


FIGURE 10 (A) Numerically reconstructed hologram when the exit pupil size is twice the size of the curved volume-holographic optical element, and (B) numerically reconstructed hologram when the exit pupil size is equal to that of the curved volume-holographic optical element.

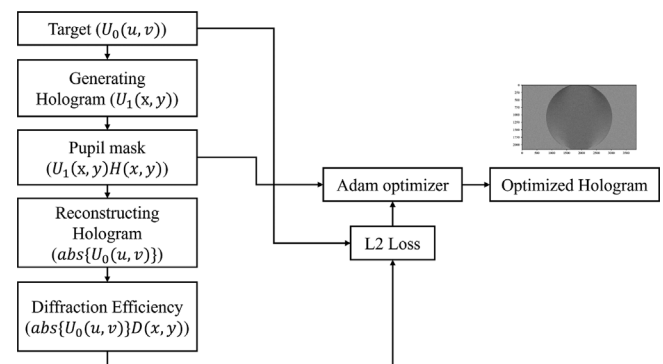


FIGURE 11 Flowchart of the computer-generated hologram (CGH) optimization for improving hologram image quality.

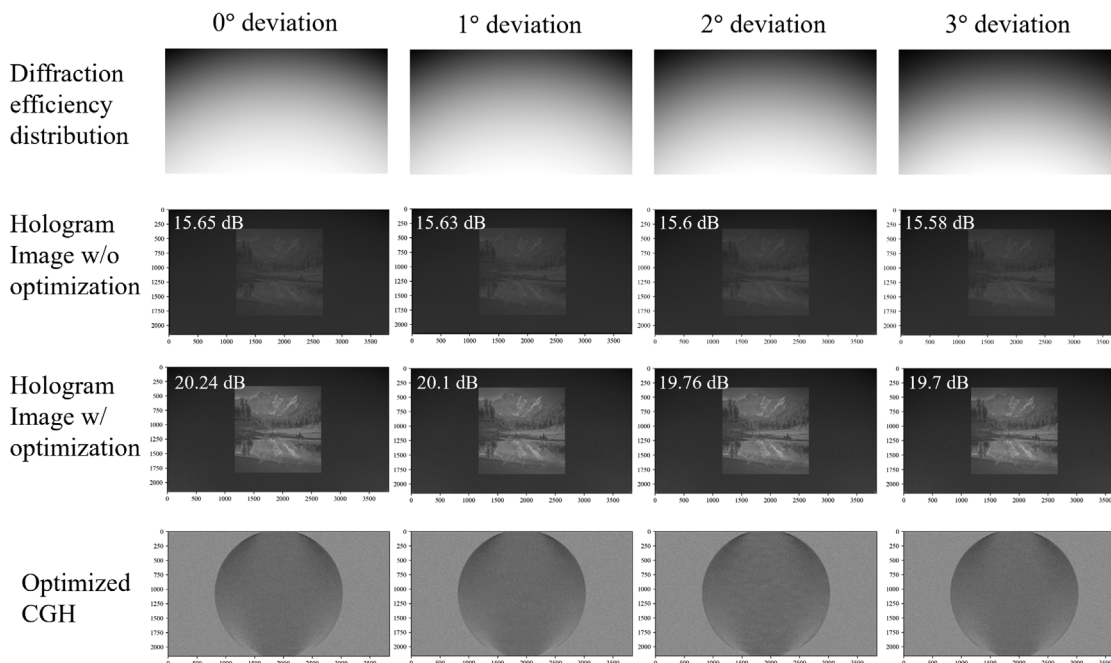


FIGURE 12 Optimization results. (First row) Diffraction efficiency distribution according to angular deviation, (second row) Reconstructed hologram image before optimization, (third row) reconstructed hologram image after optimization, and (fourth row) optimized CGH.

the hologram image becomes uniform and its quality is improved. Compared with the hologram image before optimization, the peak signal-to-noise ratio improved by more than 3 dB.

3.3 | Optical reconstruction result

To validate the proposed device, the fabricated contact lens was attached to a DSLR camera lens, as shown in Figure 9B. Subsequently, the Rubik's cube hologram was reconstructed at a distance of 1 m from the contact lens. In Figure 13, the depth of the hologram is indirectly confirmed by the blurring of the hologram image by focusing the camera on the inner and outer objects of the contact lens. However, unfortunately, the actual system exhibits a tendency for the outer regions of the overall FoV to darken due to the Gaussian distribution of light source and the spatial filter. Consequently, while the system's theoretical FoV, which is same with diffraction angle, is 15°, the supported FoV is around 10° as shown in Figure 13. Although these issues could be addressed by modifying the optical system and CGH generation algorithms, unfortunately, these issues are not deal with this study.

In addition, the contact lens produced in this study follows a structure where the HOE component (Bayfol HX-100) is inserted between two lenses which is attached by optical adhesive. In the process of adhesion, UV light

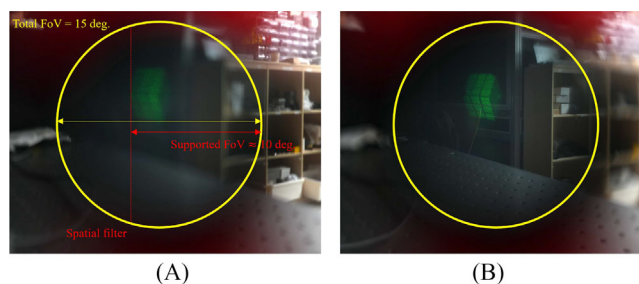


FIGURE 13 An experimentally reconstructed Rubik's cube captured (A) out-of-focus and (B) in-focus.

may enter the HOE component through internal reflection, some part of HOE cured, and it leads to a reduction in diffraction efficiency. In some cases, issues such as light leakage and dimming of external images may occur. To address these issues, more sophisticated manufacturing equipment and processes are required. This can completely resolve the problem of dimming in external images.

Typically, to implement a full-color hologram, separate optical systems for the red, green, and blue wavelengths are required, along with an optical system to combine them. This is because the V-HOE records the interference pattern of a plane wave light source at a specific wavelength, and a change in the wavelength of the incident light source alters the diffraction angle or

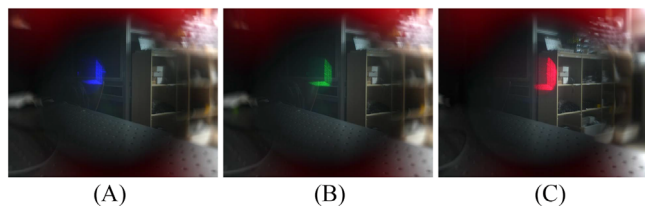


FIGURE 14 Optical reconstructed hologram image for (A) red, (B) green, and (C) blue colors.

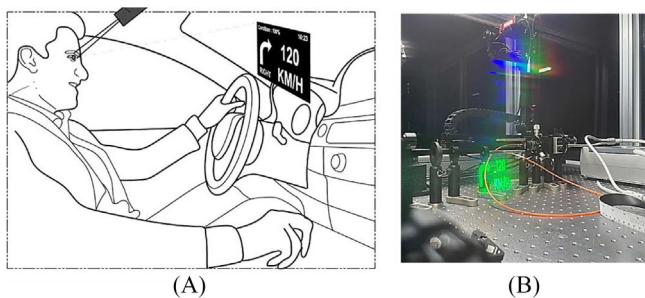


FIGURE 15 (A) Schematic of the navigation system of the proposed contact lens holographic display and (B) the captured hologram image.

efficiency. Therefore, an optical system that can correct the incident angle at each wavelength is required. However, to validate the potential of the proposed device, this study was conducted only for the G wavelength. Nevertheless, images were also captured for red and blue wavelengths, demonstrating good-quality hologram images, thereby confirming the feasibility of implementing a full-color hologram, as shown in Figure 14.

4 | CONCLUSIONS

In this study, we introduced a contact lens-type holographic AR display. The design, manufacturing, and reconstruction processes of the contact lenses were described in detail. Using the proposed concept, a FoV of 15° was achieved along with a $6.9\text{mm} \times 3.9\text{mm}$ exit pupil. To the best of our knowledge, this is a pioneering study in which holographic display technology was integrated into a contact lens. However, a notable limitation of the proposed system is its reliance on external holographic projectors. First limitation is safety. Although a laser with very low power was utilized for safety during experiment. I believe that for commercialization, through additional research is needed to explore the use of safe light sources. Second limitation is fixed eyebox. The system proposed in this study has a very small eyebox and, being fixed in a specific position, makes the holographic

image invisible when the head is moved. Thus, we currently conducting two approaches to solve this issue. Firstly, replicating the eyebox. It may introduce complexity to the optical system or require additional components, potentially leading to a reduction in the FoV in some cases. Secondly, eye-tracking system to create a dynamic eyebox that follows the observer's head moves. Considering the required eyebox size for an practical Head-Up Display (HUD) system is approximately $100\text{mm} \times 50\text{mm}$ in width and height, we anticipate that the eye-tracking system has enough performance to cover it effectively.

Despite these constraints and requirements, the proposed idea is arguably the most efficient method used for reconstructing high-resolution 3D images using contact lenses. The first target application of the proposed technology is a navigation system for automobiles as shown in Figure 15. This is because the driver's head moves within a very narrow region, and the current head-up display of automobiles suffers from problems of a small FoV and eyebox. To understand this clearly, the concept of the proposed target application and the captured hologram image are attached, as shown in Figure 14. Moreover, the viability of 3D content in monocular vision and its potential for full-color displays were successfully verified.

ACKNOWLEDGMENTS

This study was supported by an Electronics and Telecommunications Research Institute (ETRI) grant funded by the Korean government (MIST) (No. 23ZH1300) and an Institute of Information & Communications Technology Planning (IITP) grant funded by the Korean government (MSIT) (No. 2020-0-01842, Development of holographic lithography equipment and printing technology for security and books).

CONFLICT OF INTEREST STATEMENT

The author declares that there are no conflicts of interest.

ORCID

Jin Su Lee  <https://orcid.org/0000-0002-4335-9166>

REFERENCES

1. Y. Jo, C. Yoo, K. Bang, B. Lee, and B. Lee, *Eye-box extended retinal projection type near-eye display with multiple independent viewpoints*, *Appl. Opt.* **60** (2021), no. 4, A268–A276.
2. X. Duan, J. Liu, X. Shi, Z. Zhang, and J. Xiao, *Full-color see-through near-eye holographic display with 80 field of view and an expanded eye-box*, *Opt. Express* **28** (2020), no. 21, 31316–31329.
3. J. Jeong, J. Lee, C. Yoo, S. Moon, B. Lee, and B. Lee, *Holographically customized optical combiner for eye-box extended near-eye display*, *Opt. Express* **27** (2019), no. 26, 38006–38018.

4. M. Kim, S. Lim, G. Choi, Y. Kim, H. Kim, and J. Hahn, *Expanded exit-pupil holographic head-mounted display with high-speed digital micromirror device*, ETRI J. **40** (2018), no. 3, 366–375.
5. J. S. Lee, Y. K. Kim, M. Y. Lee, and Y. H. Won, *Enhanced see-through near-eye display using time-division multiplexing of a Maxwellian-view and holographic display*, Opt. Express **27** (2019), no. 2, 689–701.
6. C. Chang, K. Bang, G. Wetzstein, B. Lee, and L. Gao, *Toward the next-generation VR/AR optics: a review of holographic near-eye displays from a human-centric perspective*, Optica **7** (2020), no. 11, 1563–1578.
7. T. North, M. Wagner, S. Bourquin, and L. Kilcher, *Compact and high-brightness helmet-mounted head-up display system by retinal laser projection*, J. Display Technol. **12** (2016), no. 9, 982–985.
8. J. Chen, L. Mi, C. P. Chen, H. Liu, J. Jiang, and W. Zhang, *Design of foveated contact lens display for augmented reality*, Opt. Express **27** (2019), no. 26, 38204–38219.
9. Y. Wu, C. P. Chen, L. Mi, W. Zhang, J. Zhao, Y. Lu, W. Guo, B. Yu, Y. Li, and N. Maitlo, *Design of retinal-projection-based near-eye display with contact lens*, Opt. Express **26** (2018), no. 9, 11553–11567.
10. K. Akşit and Y. Itoh, *HoloBeam: paper-thin near-eye displays*, (IEEE Conference Virtual Reality and 3D User Interfaces (VR)), 2023, pp. 581–591.
11. J. Sano and Y. Takaki, *Holographic contact lens display that provides focusable images for eyes*, Opt. Express **29** (2021), no. 7, 10568–10579.
12. H. Kogelnik, *Coupled wave theory for thick hologram gratings*, Bell Syst. Technical J. **48** (1969), no. 9, 2909–2947.

AUTHOR BIOGRAPHY



Jin Su Lee received his BSc and MSc degrees from Korea University, and his PhD degree in electrical engineering from the Korea Advanced Institute of Science & Technology (KAIST), Daejeon, Republic of Korea. Since 2019, he has been a Senior Researcher Korea Photonics Technical Institute(KOPTI), Gwangju, Republic of Korea, from 2019 to 2022. He is now a senior researcher at the Electrical and Telecommunications Research Institute (ETRI), Daejeon, Republic of Korea. His primary research interests include holography with an emphasis on XR/AR/VR optics, freeform optics, and signal processing, as well as the development and application of advanced automotive displays and holographic technologies.

How to cite this article: J. S. Lee, *Contact lens holographic projection display based on curved volume-holographic optical element*, ETRI Journal **47** (2025), 518–526, DOI [10.4218/etrij.2023-0508](https://doi.org/10.4218/etrij.2023-0508)